

The effect of magnetic field morphology on the structure of massive IRDC clumps

Nahid Bahmani, Mohsen Nejad-Asghar

Department of Physics, University of Mazandaran, Babolsar, Iran

nejadasghar@umz.ac.ir

ABSTRACT

Infrared dark clouds (IRDCs) have dense elongated clumps and filaments with the favorable viewing condition of being on the near-side of a bright mid-infrared background. The clumps usually have multiple cores *around the center*. In this work, we study the effect of magnetic field morphology on the structure of massive IRDC clumps. To achieve this goal, we consider an axisymmetric isothermal oblate IRDC clump, embedded into a constant external magnetic field. We assume a polynomial function for the magnetic field morphology inside the clump. We use the numerical iterative methods to solve the equations: the successive over-relaxation method to find the magnetic and gravitational fluxes, and then the biconjugate gradient method to find the optimized values of mass and current densities. The results show that the IRDC clump will be very elongated along the perpendicular direction of the external magnetic field lines. Also, the assumption of choosing of a polynomial function for the magnetic field morphology leads to the formation of dense regions *around the center*. The greater the density of the central region, the larger the density of these dense regions and the closer to the center. The presence of these dense regions can lead to the formation of cores at these points.

Subject headings: ISM: structure – ISM: clouds – ISM: magnetic fields – stars: formation – (Galaxy:) local interstellar matter

1. Introduction

Infrared dark clouds (IRDCs) are cold, dense molecular clouds seen silhouetted against the bright diffuse mid-infrared emission of the Galactic plane. They were discovered during

mid-infrared imaging surveys with the Infrared Space Observatory (P  rault et al. 1996) and Midcourse Space Experiment (Egan et al. 1998). Simon et al. (2006) used 8.3 μm mid-infrared images acquired with the Midcourse Space Experiment satellite to identify and catalog IRDCs in the first and fourth quadrants of the Galactic plane. The observations show that the IRDCs have low temperatures (< 25 K), high densities ($> 10^5 \text{ cm}^{-3}$) and sizes of 1 – 10 pc (e.g., Carey et al. 1998, 2000, Butler & Tan 2009, Chira et al. 2013, Feng et al. 2016).

Many of these IRDCs have the filamentary structure with high mass non-spherical clumps on 0.01 – 1 pc size scales; two examples are G028.37+00.07 (e.g. Lim & Tan 2014) and G035.39-00.33 (e.g., Sokolov et al. 2017). The masses of these non-spherical IRDC clumps are generally of order hundreds to thousands of solar masses, and they are believed to be the precursors for formation of the massive stars and/or stellar clusters. The IRDC clumps exhibit a variety of star and cluster formation stages: from prestellar, dark, cold, and quiescent cores to active, infrared-bright and chemically rich substructures with embedded sources driving outflows and HII regions (e.g., Pillai et al. 2006, Chambers et al. 2009, Battersby et al. 2010, Sanhueza et al. 2012, Wang et al. 2011, 2014).

Most of the IRDC clumps have elongated shapes (e.g., recent report of Sanhueza et al. 2017 in the IRDC G028.23-00.19). As if a static gaseous cloud is only affected by its self-gravitational force, the spherical symmetry requires that it be a sphere. The observed non-spherical shapes like as IRDC clumps are created either by the non-static effects or by the non-symmetric forces such as the magnetic forces. The IRDC clumps are assumed to be near virial equilibrium and in approximate pressure equilibrium with the surrounding environment. A massive, virialized non-spherical IRDC clump in pressure equilibrium with its environment cannot be supported by thermal pressure, given observed temperatures of $T < 25$ K, and so must be supported by some form of non-thermal pressure, e.g., magnetic fields. The magnetic field pressure can lead to form some elongated shapes that are perpendicular to the magnetic field lines (e.g., Mouschovias 1976). Estimates of the magnetic field strengths in the IRDCs indicate values in the range 100 – 700 μG (e.g., Santos et al. 2016, Henshaw et al. 2016, Hoq et al. 2017).

The observations show that the IRDC clumps have many prestellar and protostellar cores. For example, Sanhueza et al. (2017) have recently reported some observational information about a massive elongated clump in the IRDC G028.23-00.19. This clump hosts many cores around its elongated axis (like SMA1 and SMA4 *around the center*). Hosting the cores *around the center* and along the elongated axis of the IRDC clumps may lead to the formation of non-spherical stellar clusters. Characterizing the initial conditions for formation of the stellar clusters is important for distinguishing between various theoretical

models.

Formation of the multiple cores along the major axis of a massive IRDC clump may be justified via some theoretical works that describing the fragmentation of hydrodynamic fluid cylinders (e.g., Chandrasekhar and Fermi 1953, Tomisaka 1995, Hernandez and Tan 2011, Contreras et al. 2016). Henshaw et al. (2016) investigated the spatial distribution of the cores along the major axis of the IRDC G035.39-00.33. They found a significant discrepancy between the observed distribution of the cores, and that predicted by the theoretical works, which used the fragmentation of hydrodynamic fluid cylinders. Also, these theoretical models cannot justify the distribution of the cores *around the center* of an IRDC clump. Can the presence of a magnetic field through the IRDC clump, in addition to its force for formation of non-spherical shape, also justify some constraints on the spatial positions of the cores in them? Here, we want to present a theoretical model for imprint of the morphology of the magnetic field lines to justify formation of the cores through elongated axis (and *around the center*) of a massive IRDC clump. For this purpose, the formulation of the theoretical model is given in § 2. The boundary conditions and the morphology of the magnetic field is given in §3. The results are presented at §4, and section 5 is devoted to a summary and conclusions.

2. Formulation of the problem

We consider a nearly spherical (oblate) massive IRDC clump, which is in the isothermal state with sound speed c_s . We use axisymmetric cylinder polar coordinate (ϖ, z) , centered on the origin of this IRDC clump. The magnetic field is assumed to be uniform in the outer regions of the clump. The z direction is considered along this uniform magnetic field. We must consider a suitable morphology of the magnetic field in the inner regions of the IRDC clump. The schematic diagram of the shape of the IRDC clump and its magnetic field configuration is shown in the Fig. 1.

The Φ_B is the magnetic flux contained within the surface generated by rotating any magnetic field line about the z -axis (Fig. 1). The relation $\nabla \cdot \mathbf{B} = 0$ allows us to recast \mathbf{B} in terms of the magnetic potential \mathbf{A} (i.e., $\mathbf{B} = \nabla \times \mathbf{A}$). The vector field \mathbf{A} need have only a nonzero ϕ -component in order to generate an arbitrary poloidal \mathbf{B} -field. If S be any circular two-dimensional surface centered on the z -axis and bounded by a circle of radius ϖ , then $\Phi_B = \int_S (\nabla \times \mathbf{A}) \cdot \hat{k} da = 2\pi\varpi A_\phi$. Employing the unit vector \hat{e}_ϕ , we write

$$\begin{aligned} \mathbf{B} &= \nabla \times (A_\phi \hat{e}_\phi) \\ &= -\frac{\hat{e}_\phi}{\varpi} \times \nabla(\varpi A_\phi) \end{aligned}$$

$$= -\frac{\hat{e}_\phi}{2\pi\varpi c} \times \nabla\Phi_B. \quad (1)$$

By using of Ampere's law $\nabla \times \mathbf{B} = \frac{4\pi}{c}\mathbf{j}$ and equation (1), we obtain the magnetic induction equation as

$$\frac{\partial}{\partial\varpi} \left(\frac{1}{\varpi} \frac{\partial\Phi_B}{\partial\varpi} \right) + \frac{1}{\varpi} \frac{\partial^2\Phi_B}{\partial z^2} = -\frac{8\pi^2}{c} j_\phi, \quad (2)$$

where j_ϕ is the ϕ -component of current density.

The equation for force balance is

$$0 = -c_s^2 \nabla\rho - \rho \nabla\Phi_g + \frac{1}{c} \mathbf{j} \times \mathbf{B}, \quad (3)$$

where Φ_g is the gravitational potential

$$\frac{1}{\varpi} \frac{\partial}{\partial\varpi} \left(\varpi \frac{\partial\Phi_g}{\partial\varpi} \right) + \frac{\partial^2\Phi_g}{\partial z^2} = 4\pi G\rho. \quad (4)$$

With poloidal magnetic field and toroidal current density, the magnetic force per unit volume, $\frac{1}{c}\mathbf{j} \times \mathbf{B}$, must be a poloidal vector with both ϖ and z components. In the this way, the force balance equation (3) can be rewritten as

$$c_s^2 \frac{\partial\rho}{\partial\varpi} + \rho \frac{\partial\Phi_g}{\partial\varpi} = \frac{j_\phi}{2\pi\varpi c} \frac{\partial\Phi_B}{\partial\varpi}, \quad (5)$$

$$c_s^2 \frac{\partial\rho}{\partial z} + \rho \frac{\partial\Phi_g}{\partial z} = \frac{j_\phi}{2\pi\varpi c} \frac{\partial\Phi_B}{\partial z}. \quad (6)$$

We use the scale values of length, temperature, and density equal to $[l] = 1 \text{ pc}$, $[T] = 10 \text{ K}$, $[\rho] = 2m_H \times (10^4 \text{ cm}^{-3})$, respectively, so that the scale of magnetic field strength is $[B] = 18.6 \mu\text{G}$ and the mass scale is $[M] = 9850 M_\odot$. Using these scale units, the basic equations for the axisymmetric massive isothermal IRDC clump in the force balance equilibrium can be rewritten as

$$\frac{\partial}{\partial\varpi} \left(\frac{1}{\varpi} \frac{\partial\Phi_B}{\partial\varpi} \right) + \frac{1}{\varpi} \frac{\partial^2\Phi_B}{\partial z^2} = -j_\phi, \quad (7)$$

$$\frac{1}{\varpi} \frac{\partial}{\partial\varpi} \left(\varpi \frac{\partial\Phi_g}{\partial\varpi} \right) + \frac{\partial^2\Phi_g}{\partial z^2} = \rho, \quad (8)$$

$$\frac{\partial\rho}{\partial\varpi} + \rho \frac{\partial\Phi_g}{\partial\varpi} = \frac{j_\phi}{\varpi} \frac{\partial\Phi_B}{\partial\varpi}, \quad (9)$$

$$\frac{\partial\rho}{\partial z} + \rho \frac{\partial\Phi_g}{\partial z} = \frac{j_\phi}{\varpi} \frac{\partial\Phi_B}{\partial z}. \quad (10)$$

For solving these equations and determining the internal profile structure of an IRDC clump, we need to know the boundary values (i.e., values of ρ , j_ϕ , Φ_B , and Φ_g on the dash lines 1–4 of Fig. 1).

3. Values in the boundaries

We consider an isothermal IRDC clump with temperature $T \approx 1 [T]$ and total mass $M \approx 0.15 [M]$. The clump is embedded in the inter-clump medium of IRDC. The inter-clump medium is assumed to have density $\rho_{int} \approx 1 [\rho]$ and uniform magnetic field $B_{int} \approx 8.5 [B]$. These values are typically correspond to the MM1 clump through the IRDC G28.23-00.19 (Sanhueza et al. 2017, Hoq et al. 2017). The radii of the clump in the z -axis and ϖ -axis directions are R_0 and λR_0 , respectively, where $\lambda > 1$ is the oblate axis ratio. For simplicity, we assume that the boundaries at one quadrant of $\varpi - z$ plane, are given as four lines 1 – 4, as depicted in the Fig. 1.

In boundary line 1 with $(\varpi = 0, z)$, the j_ϕ and Φ_B are zero so that the equation (10) imply that $\rho = \rho_c \exp(-\Phi_g)$, where ρ_c is the central density in unit of $[\rho]$. Here, we assume that the density on this boundary line is corresponded with the profile of an infinite layer. In the assumption of infinite layer, the gravitational potential is independent of ϖ so that the equation (8) becomes

$$\frac{d^2\Phi_g}{dz^2} = \rho_c \exp(-\Phi_g). \quad (11)$$

This equation can be solved numerically with boundary conditions $\Phi_{g(\varpi=0, z=0)} = 0$ and $\frac{d\Phi_g}{dz}|_{(\varpi=0, z=0)} = 0$. By choosing each value for $\rho_c > \rho_{int}$, there is a special value for R_0 in which the density at $z = R_0$ will be equal to ρ_{int} . The maximum allowed radius of the IRDC clump in the z -axis direction, R_0 , for different values of the central density, ρ_c , is shown in the Fig. 2. The density contrast, ρ_c/ρ_{int} , greater than 3.5 causes to contract the layer in the z -axis direction due to the importance of the self-gravitational force. Counterpart of this case, in the spherically symmetric clouds, is known as the occurrence of gravitational instability (i.e., Bonnor-Ebert spheres, see, e.g., Stahler and Palla 2004, Fig. 9.2 for isothermal case, Nejad-Asghar 2016, Fig. 3 for non-isothermal cases). Here, we choose the boundary line 4 being near the maximum allowed value of R_0 (i.e., $Z_\infty \approx 0.94$). To consider the oblateness of the IRDC clump and departure from infinite layer approximation, we will approximately consider the term $\frac{1}{\varpi} \frac{\partial}{\partial \varpi} \left(\varpi \frac{\partial \Phi_g}{\partial \varpi} \right)$, and reevaluate the R_0 , in each iterative process as mentioned in the next section.

In boundary line 2 with $(\varpi, z = 0)$, we assume the density and the magnetic field strength are corresponded with the profiles of an infinite cylinder. In the assumption of infinite cylinder, the quantities Φ_g , ρ , j_ϕ , and Φ_B are independent of z so that the basic equations (7)-(10) reduce to

$$\frac{d^2\rho}{d\varpi^2} + \left(\frac{1}{\varpi} + \frac{f}{\rho} \right) \frac{d\rho}{d\varpi} - \frac{1}{\rho} \left(\frac{d\rho}{d\varpi} \right)^2 + \rho^2 = \frac{f}{\varpi} + \frac{df}{d\varpi}, \quad (12)$$

where $f \equiv 2\pi j_\phi B$. Knowing the magnetic field B in this boundary line, the magnetic flux

and current density can be obtained via $\Phi_B = \int_0^\varpi 2\pi\varpi' B d\varpi'$ and $j_\phi = -2\pi \frac{dB}{d\varpi}$, respectively. If we choose a suitable model for the magnetic field B , the equation (12) can be solved numerically with boundary conditions $\rho_{(\varpi=0,z=0)} = \rho_c$ and $\frac{d\rho}{d\varpi}|_{(\varpi=0,z=0)} = 0$. The oblate axis ratio λ is identified so that $\rho_{(\varpi=\lambda R_0,z=0)} = \rho_{int}$. Then, the gravitational potential can be obtained from equation (9) as $\Phi_g = -\ln \frac{\rho}{\rho_c} + \int_0^\varpi \frac{f}{\rho} d\varpi'$.

The most important thing in the boundary line 2 is the morphology of the magnetic field. We do not have enough observational information about the magnetic field strengths through the sub-pc scales of the IRDC clumps (Hoq et al. 2017). We assume that the magnetic field at the center of the IRDC clump is $(1+\eta)B_{int}$ where η is the fractional change of the magnetic field strength at the central region. If we use a power law relation (i.e., $B \propto \rho^\kappa$) between the central magnetic field strength and the central density (Crutcher 2012), we have $\eta = \left(\frac{\rho_c}{\rho_{int}}\right)^\kappa - 1$. Here, we choose $\kappa \approx 0.3$ (Nejad-Asghar 2016). Here, we consider a polynomial function for the magnetic field morphology. The first term that justify the condition $j_\phi = -2\pi \frac{dB}{d\varpi}|_{(\varpi=0,z=0)} = 0$ is the quadratic term as $B_{(\varpi,z=0)} = B_{int} \times [(1+\eta) - a_2\varpi^2]$, where the coefficient $a_2 \geq 0$ determines the slope of decreasing of the magnetic field by moving away from the center. Since the slope is negative, the magnetic force is in the positive ϖ direction. This force implies that a pressure gradient must be occurred so that the force balance (3) be justified. In the absence of magnetic field, the force balance between the gravitational force and pressure gradient lead to decreasing of pressure (and also decreasing of density in the isothermal case) by moving away from the center. The magnetic force is in the inverse direction of the gravitational force, thus, considering of the magnetic field morphology with greater negative slopes (i.e., grater values of a_2) can lead to increasing of the pressure (and also density) by moving away from the center. Solution of the equation (12), near the origin, for different values of a_2 are shown in Fig. 3. The next boundary conditions on the magnetic strength are $j_\phi(\varpi=\lambda R_0,z=0) = 0$ and $\Phi_{B(\varpi=\lambda R_0,z=0)} = \pi(\lambda R_0)^2 B_{int}$. Considering the next next term of the polynomial function (i.e., cubic term) leads to choosing the magnetic morphology as

$$B_{(\varpi,z=0)} = B_{int} \times \left[(1+\eta) - \frac{10}{7} \left(3\eta \frac{\varpi^2}{\lambda^2 R_0^2} - 2\eta \frac{\varpi^3}{\lambda^3 R_0^3} \right) \right]. \quad (13)$$

In the region $\varpi > \lambda R_0$, the magnetic field will increase slowly to reach the inter-clump value B_{int} . This region is not important for us.

In boundary lines 3 and 4, which are assumed to be at the inter-clump medium, we have $\rho = \rho_{int}$ and $j_\phi = 0$. The magnetic flux at the boundary line 3 is $\Phi_B = \pi(\lambda R_0)^2 B_{int}$ and at the boundary line 4 is $\Phi_B = \pi\varpi^2 B_{int}$. For gravitational potential, Mouschovias (1976) used a point mass approximation located at the origin of coordinates. Since, oblateness of a spherical mass gives it a nonzero quadrupole moments (e.g., Fitzpatrick 2012), here we add

the quadrupole approximation as

$$\Phi_{g(\varpi,z)} = J_0 \frac{M}{(z^2 + \varpi^2)^{\frac{1}{2}}} + J_2 \frac{MR_0^2}{(z^2 + \varpi^2)^{\frac{3}{2}}}, \quad (14)$$

where J_0 and J_2 are chosen so that the continuity of the gravitational potential being established at the intersection of boundary lines 1 and 4, i.e., $(\varpi = 0, z = Z_\infty)$, and the intersection of boundary lines 2 and 3, i.e., $(\varpi = \lambda R_0, z = 0)$. If Φ_{g14} is the result of gravitational potential at $(\varpi = 0, z = Z_\infty)$ obtained from integration across the boundary line 1, and Φ_{g23} is the result of gravitational potential at $(\varpi = \lambda R_0, z = 0)$ obtained from integration across the boundary line 2, we have

$$J_0 = \frac{1}{\lambda^2 - \alpha^2} \frac{(\lambda^3 \Phi_{g23} - \alpha^3 \Phi_{g14}) R_0}{M},$$

$$J_2 = -\frac{\alpha^2 \lambda^2}{\lambda^2 - \alpha^2} \frac{(\lambda \Phi_{g23} - \alpha \Phi_{g14}) R_0}{M},$$

where $\alpha \equiv Z_\infty / R_0$.

4. Results

In the previous section, the boundary values are specified around the edge of the rectangular grid. In the interior points, the equations (7)-(10) must be satisfied. We consider these equations by the finite-difference method, and employ an iterative process to find the values of ρ , Φ_g , j_ϕ and Φ_B at the internal grid points.

First, we consider the equations (7) and (8) with assumption that the values of ρ and j_ϕ are known at the all (i.e., known fixed values at boundaries and assumed guessed values at internal) grid points. The best initial guess for ρ and j_ϕ , at an internal point (i, j) , is a linear functional form as

$$f_{i,j} = f_{i,1} + \frac{f_{i,N} - f_{i,1}}{Z_\infty} z_j, \quad (15)$$

where f corresponds to ρ and j_ϕ , and the integer numbers i (corresponding to the ϖ -axis) and j (corresponding to the z -axis) run from 2 to a maximum value $N - 1$. The finite difference of the equations (7) and (8), on the rectangular grid, is an equation of the form

$$a_{i,j} u_{i+1,j} + b_{i,j} u_{i-1,j} + c_{i,j} u_{i,j+1} + d_{i,j} u_{i,j-1} + e_{i,j} u_{i,j} = f_{i,j}, \quad (16)$$

where u corresponds to Φ_B and Φ_g , and the coefficients a , b , c , d and e are all known values on the internal grid points. We use the successive-over-relaxation (SOR) method (Press et

al. 2007) to solve the equation (16), and to find the values of Φ_B and Φ_g on the internal grid points.

Now, we turn our attention to the equations (9) and (10) to find some best estimated new values for ρ and j_ϕ . Eliminating j_ϕ between (9) and (10) leads to a finite difference equation for density ρ as follows

$$\frac{f_{i,j}^{Bz}}{2\Delta\varpi}\rho_{i+1,j} - \frac{f_{i,j}^{Bz}}{2\Delta\varpi}\rho_{i-1,j} - \frac{f_{i,j}^{B\varpi}}{2\Delta z}\rho_{i,j+1} + \frac{f_{i,j}^{B\varpi}}{2\Delta z}\rho_{i,j-1} + (f_{i,j}^{Bz}f_{i,j}^{g\varpi} - f_{i,j}^{B\varpi}f_{i,j}^{gz})\rho_{i,j} = 0, \quad (17)$$

where Δz and $\Delta\varpi$ are the grid sizes in the z and ϖ axes, respectively, and

$$\begin{aligned} f_{i,j}^{B\varpi} &\equiv \left(\frac{\partial\Phi_B}{\partial\varpi} \right)_{i,j}, & f_{i,j}^{Bz} &\equiv \left(\frac{\partial\Phi_B}{\partial z} \right)_{i,j}, \\ f_{i,j}^{g\varpi} &\equiv \left(\frac{\partial\Phi_g}{\partial\varpi} \right)_{i,j}, & f_{i,j}^{gz} &\equiv \left(\frac{\partial\Phi_g}{\partial z} \right)_{i,j}, \end{aligned}$$

must be evaluated (via smoothed finite difference method) with the new obtained (via SOR method) values of Φ_B and Φ_g on the internal grid points. Numbering the two dimensions of grid points in a single one-dimensional sequence by $l = (i - 2)(N - 2) + (j - 1)$, equation (17) takes the matrix form $\mathbf{Ax} = \mathbf{b}$ where \mathbf{A} is a sparse matrix similar to the Fig. 19.0.3 of Press et al. (2007). We use the biconjugate gradient method (the routine LINBCG of Press et al. 2007 that is derived from a set of iterative routines originally written by Anne Greenbaum) to solve this set of linear algebraic equations with sparse matrix. Now, knowing the density in all grid points, the current density can be obtained via

$$j_{\phi i,j} = \frac{\varpi_i}{f_{i,j}^{B\varpi}} \left(\frac{\rho_{i+1,j} - \rho_{i-1,j}}{2\Delta\varpi} + f_{i,j}^{g\varpi} \rho_{i,j} \right). \quad (18)$$

We use the new obtained values of ρ and j_ϕ to iterate the procedure of solving the equation (16) via SOR, and then obtaining new values of ρ and j_ϕ via equations (17) and (18). This iterative method generates a sequence of improved solutions for ρ and j_ϕ . The isodensity contours are displayed in the Fig. 4 for two values of the central density $\rho_c = 2$ and 5.

5. Summary and conclusion

In this work, we investigated the effect of the magnetic field morphology on the structure of the massive IRDC clumps. To achieve this goal, we constructed the fundamental equations for an axisymmetric isothermal oblate IRDC clump, embedded into a constant external

magnetic field, so that the external field is assumed to be along the z axis of the cylindrical polar coordinates. As shown schematically in the Fig. 1, the radii of the clump in the direction of the z and ϖ axes are R_0 and λR_0 , respectively, where $\lambda > 1$ is the oblate axis ratio. For simplicity, we assume that the boundaries at one quadrant of $\varpi - z$ plane, are specified as four lines 1 – 4, as depicted in the Fig. 1. To solve these equations, we need the boundary value conditions.

We assumed that the density on the boundary line 1 is corresponded with the profile of an infinite layer. In the assumption of infinite layer, the values of R_0 versus different values of the central density, ρ_c , is depicted in the Fig. 2. Similar to the Bonnor-Ebert spheres in the spherical cases, the density contrast, ρ_c/ρ_{int} , greater than 3.5 causes to contract the layer in the z -axis direction due to the importance of the self-gravitational force. To consider the oblateness of the IRDC clump and departure from infinite layer approximation, we approximately considered the term $\frac{1}{\varpi} \frac{\partial}{\partial \varpi} \left(\varpi \frac{\partial \Phi_g}{\partial \varpi} \right)$, and reevaluate the R_0 , in each iterative process.

In boundary line 2, we assume the density and the magnetic field strength are corresponded with the profiles of an infinite cylinder. Here, we need a magnetic field morphology. We considered a polynomial function for the magnetic field morphology. Decreasing of the magnetic field by moving away from the center implies that the magnetic force be in the inverse direction of the gravitational force so that the pressure (and also density) increases as shown in the Fig. 3. Here, we chose the magnetic morphology as given by polynomial equation (13) which appropriately justify the boundary conditions.

Boundary lines 3 and 4 are located at the inter-clump medium. With known boundary value conditions on these four lines, we solved equations (7) and (8), with the successive-over-relaxation method, to obtain Φ_g and Φ_B . Then, we used the obtained values of Φ_g and Φ_B to solve the equations (9) and (10), with the biconjugate gradient method, to find new values of ρ and j_ϕ . Then, we put these values in equations (7) and (8) and iterate this process. In Fig. 4, the isodensity is plotted for two values of the central density $\rho_c = 2$ and 5.

In both diagrams of Fig. 4, we see that, firstly, the IRDC clump is very elongated along the perpendicular direction of the external magnetic field lines. Secondly, the choice of the magnetic field morphology (13) leads to the formation of dense regions around the center. The greater the density of the central region, the larger the density of these dense regions and the closer to the z axis. The presence of these dense regions can lead to the formation of cores at these points. These results are somewhat consistent with the results of figure 1 of Sanhueza et al. (2017), who has found multiple cores near the elongated axis and *around the center* of the massive clump of IRDC G028.23-00.19.

We have shown that by choosing the appropriate morphology for the magnetic field, we can justify the presence of the multiple cores *around the center* and near the elongated axis of the IRDC clump G028.23-00.19. In fact, for the general conclusion, not only the magnitude and direction of the magnetic field within the clumps of IRDCs must be investigated via suitable methods (e.g., techniques outlined by Hoq et al. 2017), but also must be searched for in the multiple cores within them via suitable observational techniques (e.g., methods outlined by Sanhueza et al. 2017). The oblate structure of the massive clump of IRDC G028.23-00.19 (with dense regions *around the center* and along its elongated axis), obtained from magnetic morphology (13), may also be appropriate for clumps of other IRDCs. Increasing new observational information from inside of the IRDC clumps (i.e., magnetic field and positions of dense regions through it), may help us to select other morphologies for the magnetic field. In any way, the morphology of the magnetic field affects on the sub-structure of the massive IRDC clumps. We need more observational information from inside of the IRDC clumps to completely deduce a suitable concluding remark for choosing an appropriate morphology for the magnetic field.

REFERENCES

- Battersby, C., Bally, J., Jackson, J. M., Ginsburg, A., Shirley, Y. L., Schlingman, W., Glenn, J., 2010, ApJ, 721, 222
- Butler, M. J. & Tan, J. C. 2009, ApJ, 696, 484
- Carey, S. J., Clark, F. O., Egan, M. P., et al. 1998, ApJ, 508, 721
- Carey, S. J., Egan, M. P., Kuchar, T. A., Mizuno, D., Feldman, P. A., Redman, R. O., Price, S. D., 2000, 197th AAS Meeting, Bulletin of the American Astronomical Society, Vol. 32, p. 1396
- Chambers, E. T., Jackson, J. M., Rathborne, J. M., Simon, R., 2009, ApJ, 181, 360
- Chandrasekhar, S., Fermi, E., 1953, ApJ, 118, 116
- Chira R.A., Beuther H., Linz H., Schuller F., Walmsley C. M., Menten K. M., Bronfman L., 2013, A&A, 552, 40
- Contreras, Y., Garay, G., Rathborne, J. M., Sanhueza, P., 2016, MNRAS, 456, 2041
- Crutcher, R.M., 2012, ARA&A, 50, 29

- Egan M. P., Shipman R. F., Price S. D., Carey S. J., Clark F. O., Cohen M., 1998, ApJ, 494, 199
- Feng, S., Beuther, H., Zhang, Q., Henning, Th., Linz, H., Ragan, S., Smith, R., 2016, A&A, 592, 21
- Fitzpatrick, R., 2012, *An Introduction to Celestial Mechanics*, Cambridge University Press
- Henshaw, J. D., Caselli, P., Fontani, F., Jiménez-Serra, I., Tan, J. C., Longmore, S. N., Pineda, J. E., Parker, R. J., Barnes, A. T. 2016, MNRAS, 463, 146
- Hernandez, A. K., Tan, J. C., 2011, ApJ, 730, 44
- Hoq, S., Clemens, D. P., Guzmán, A. E., Cashman, L., R., 2017, APJ, 836, 199
- Lim, W., Tan, J. C., 2014, ApJ, 780, 29
- Mouschovias, T. C. H., 1976, APJ, 206, 753
- Nejad-Asghar, M., 2016, Ap&SS, 361, 384
- Pérault, M. et al., 1996, A&A, 315, 165
- Pillai, T., Wyrowski, F., Carey, S. J., Menten, K. M., 2006, A&A, 450, 569
- Press, W.H., Teukolsky, S.A., Vetterling, W.T., Flannery, B.P., 2007, *Numerical recipes in FORTRAN. The art of scientific computing*, 3rd ed., New York: Cambridge University Press
- Sanhueza, P., Jackson, J. M., Foster, J. B., Garay, G., Silva, A., Finn, S., C. 2012, ApJ, 756, 60
- Sanhueza, P., Jackson, J. M., Zhang, Q., Guzmán, A. E., Lu, X, Stephens, I. W., Wang, K., Tatematsu, K., 2017, ApJ, 841, 97
- Santos, F.P., Busquet, G., Franco, G.A.P., Girat, & J.M., Zhang, Q., 2016, ApJ, 832, 186
- Simon, R., Jackson, J. M., Rathborne, J. M. & Chambers, E. T., 2006, ApJ, 639, 227
- Sokolov, V., Wang, K., Pineda, J. E., Caselli, P., Henshaw, J. D., Tan, J. C., Fontani, F., Jiménez-Serra, I., Lim, W., 2017, arXiv170608903
- Stahler, S.W., Palla, F., 2004, *The Formation of Stars*, WILEY-VCH Verlag GmbH & Co. KGaA, Weinheim

Tomisaka, K., 1995, ApJ, 438, 226

Wang, K.; Zhang, Q., Wu, Y., Zhang, 2011, ApJ, 735, 64

Wang, K., Zhang, Q., Testi, L., van der Tak, F., Wu, Y., Zhang, H., Pillai, T., Wyrowski, F., Carey, S., Ragan, S. E., Henning, T., 2014, MNRAS, 439, 3275

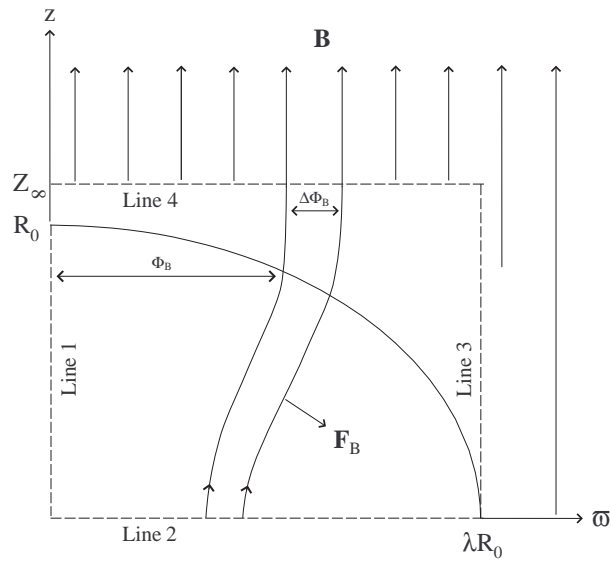


Fig. 1.— One quadrant of a magnetically supported nearly spherical (oblate with axis ratio λ) IRDC clump. The field curvature creates an outward magnetic force, as shown. The boundaries are depicted by dash lines 1 – 4, and the magnetic field in the outer regions are assumed to be uniform. Φ_B is the magnetic flux contained within the surface generated by rotating any field line about the z -axis.

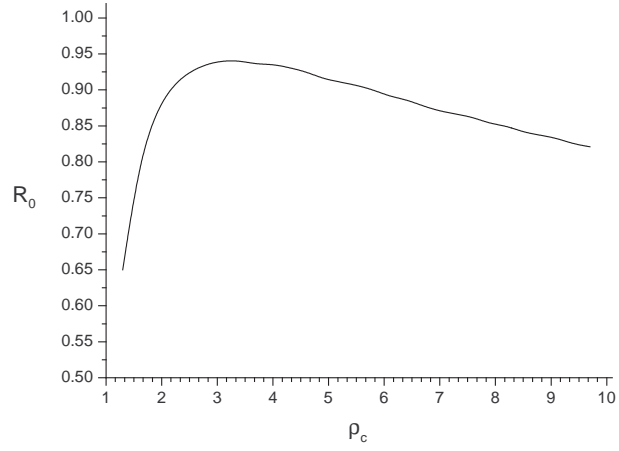


Fig. 2.— Radius of the IRDC clump in the z -axis direction for different values of the central density. The density at $z = R_0$ must be equal to the inter-clump density $\rho_{int} = 1[\rho]$.

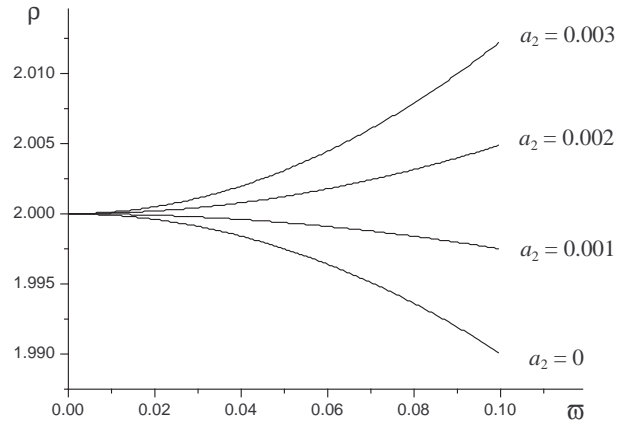
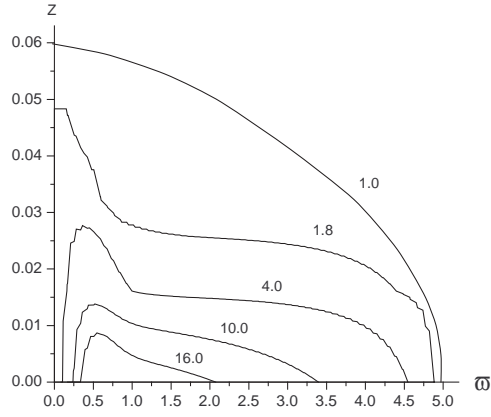
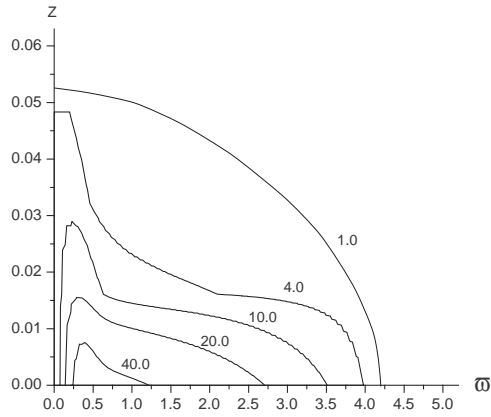


Fig. 3.— Density near the origin of the boundary line 2, with magnetic field morphology $B_{(\varpi, z=0)} = B_{int} \times [(1 + \eta) - a_2 \varpi^2]$.



(a)



(b)

Fig. 4.— Isodensity contours for one quadrant of IRDC clump with (a) $\rho_c = 2$ and (b) $\rho_c = 5$.